Eur. Phys. J. C (2025) 85:79
https://doi.org/10.1140/epjc/s10052-024-13735-0

THE EUROPEAN PHYSICAL JOURNAL C

Regular Article - Theoretical Physics

Constructing stellar solutions with spherical symmetry through quadratic anisotropy in $f(Q)$ gravity

R. Kumar[1,a], **S. K. Maurya**[2,b], **A. Errehymy**[3,c], **A. Jaiswal**[1,4,d], **K. Myrzakulov**[5,e], **S. Sharma**[1,f]

[1] Department of Mathematics and Statistics, Deen Dayal Upadhyaya Gorakhpur University, Gorakhpur, India
[2] Department of Mathematical and Physical Sciences, College of Arts and Sciences, University of Nizwa, Nizwa 616, Oman
[3] Astrophysics Research Centre, School of Mathematics, Statistics and Computer Science, University of KwaZulu-Natal, Private Bag X54001, Durban 4000, South Africa
[4] Pacif Institute of Cosmology and Selfology (PICS), Sagara, Sambalpur, Odisha 768224, India
[5] Department of General and Theoretical Physics, L.N. Gumilyov Eurasian National University, Astana 010008, Kazakhstan

Received: 23 September 2024 / Accepted: 26 December 2024

Abstract This article examines anisotropic models to characterize compact stars (CSs) in the context of modified $f(Q)$ gravity theory. To achieve this, we employ the linear functional form $f(Q) = \alpha Q + \beta$. A physically meaningful metric potential g_{rr} is considered, and a quadratic form of anisotropy is utilized to solve the Einstein field equations in closed form. This class of solutions is then applied to characterize observed pulsars from various perspectives. In the scope of $f(Q)$ gravity, we address the Darmois–Israel junction requirements to guarantee a smooth matching of the inner metric with the external metric (Schwarzschild (Anti-) de Sitter solution) at the boundary hypersurface. By applying these junction conditions, we determine the model parameters involved in the solutions. Additionally, this study evaluates the physical viability and dynamical stability of the solution for different values of the $f(Q)$-parameter α within the compact star (CS). The mass–radius relationships associated with observational constraints are analyzed for several compact stars, including Vela X-1, PSR J1614-2230, and PSR J0952-0607. The investigation indicates that the estimated radius of the compact object PSR J0952-0607, with mass $2.35 \pm 0.17\ M_{\odot}$, is around $15.79^{+0.05}_{-0.09}$ km for a particular parameter value of $\alpha = 2.0$, and the moment of inertia for the de Sitter space is determined as 4.31×10^{45} g cm^2. The $I - M$ curve shows greater sensitivity to the stiffness of the equation of state than the $M - R$ curve, reinforcing our conclusion about the $I - M$ framework's responsiveness. Finally, we predicted the corresponding radii and moments of inertia for various values of α based on the $M - R$ and $M - I$ curves.

Contents

[a] e-mail: rajesh.mathstat@ddugu.ac.in
[b] e-mail: sunil@unizwa.edu.om
[c] e-mail: abdelghani.errehymy@gmail.com (corresponding author)
[d] e-mail: annujais3012@gmail.com
[e] e-mail: krmyrzakulov@gmail.com (corresponding author)
[f] e-mail: shubhamddugu@gmail.com

Published online: 25 January 2025

1 Introduction

The theory of general relativity (GR) has been groundbreaking, yet it encounters difficulties in accounting for the universe's late-time acceleration, the existence of dark matter, and the quantization of gravitational interactions. Significant gaps in our understanding of gravitational theory persist, particularly in addressing these challenges. To explain the late-time acceleration of the universe, it is essential to consider the possibility of dark energy or a modification of gravity. Consistency with GR requires that space-time be Levi-Civita, and Riemannian geometry is typically used to define an affine connection. However, the use of affine connections in GR has its limitations. Exploring different affine connections with alternative descriptions of gravity could help bridge this disparity in research [1–3]. This exploration underscores the need for alternative theories of gravity, such as modified gravity theories. Promising approaches include $f(\mathcal{R})$ gravity, $f(T)$ gravity, $f(\mathcal{R}, T)$ gravity, $f(Q)$ gravity, and others, offering diverse frameworks for further investigation in future studies [4–16].

The $f(\mathcal{R})$ theory offers a promising approach to overcoming the limitations of GR. By modifying the scalar curvature R in the Lagrangian, $f(\mathcal{R})$ gravity has demonstrated significant potential in explaining dark energy, as highlighted in [17–19]. In GR, the affine connection permits a nonzero curvature $\mathcal{R}$, while nonmetricity Q and torsion T can be set to zero, similar to the construction of $f(T)$ gravity. Various theories and geometries can be developed where nonmetricity, curvature, and torsion take on different values, either zero or non-zero. Specifically, in $f(T)$ gravity, curvature and nonmetricity are set to zero, leading to a symmetric teleparallel formulation of general relativity (STGR). Numerous studies have explored STGR, as referenced in [20–26]. In $f(Q)$ gravity, the gravitational Lagrangian includes an arbitrary function of nonmetricity. A significant advantage of $f(Q)$ gravity is that its field equations are second-order, unlike the fourth-order differential equations encountered in $f(\mathcal{R})$ theory. This study primarily focuses on $f(Q)$ gravity. This modified gravity framework provides a clear formulation of classical GR without incorporating the affine structure of spacetime, thereby enhancing inertial gravitational interactions. Notably, $f(Q)$ gravity can account for the late-time acceleration of the universe without requiring modifications to scalar fields [27–29]. Various fields have been explored to assess the viability of the $f(Q)$ gravity model [30–33]. Alternative approaches to modified gravity theories have also been investigated, such as a bouncing model proposed in [34]. Additionally, research on holographic dark energy has employed the functional form $f(Q) = Q + Q^n$ [35]. This investigation found that, when solving for a static CS solution, no Schwarzschild analog solution exists in the context of a non-vanishing $f(Q)$ function [28].

In the teleparallel equivalent of general relativity (TEGR), although it is less well-known, it is formulated equivalently to GR and symmetric teleparallel general relativity (STGR). A key distinction in STGR is that both curvature and torsion are set to zero, with gravity attributed to the nonmetricity $Q_{\alpha\mu\nu}$. Like the conditions of zero torsion and nonmetricity, a coincident gauge can always be applied [21]. A notable aspect of this approach is the vanishing of the affine connection. However, when continuing to employ the coincident gauge [36–38] and considering the metric as the only fundamental variable in modified STGR theories, such as $f(Q)$ theory, the behavior of metrics will differ across various coordinate systems. Furthermore, the influence of anisotropy on the macroscopic properties of stellar structures such as mass, radius, moment of inertia, tidal deformability, and nonradial oscillations is explored in the following works, See Refs. [39–44]. Herrera and Santos [45] have extensively studied anisotropic fluid spheres in GR, suggesting that this anisotropy likely persists in the system's final equilibrium state. Indeed, no known physical process within a compact star can reverse the pressure anisotropy developed during its dynamical evolution. Therefore, the principal pressures within the compact star should generally be unequal. Jeans [46] investigated the anisotropy in the distribution of stars within a galaxy exhibiting spherical symmetry. However, Lemaitre [47] was the first to address local anisotropy in the context of GR. Numerous studies have since explored anisotropic solutions for relativistic stars, beginning with the pioneering work by researchers [48,49], who extended Einstein's field equations to higher dimensions ($n \geq 4$) in their model of an anisotropic star. In a subsequent paper [50], these researchers derived an exact solution for an anisotropic star by assuming specific forms of anisotropy. Gleiser and Dev [51] later proposed a new exact solution for an anisotropic star and examined the star's stability using Chandrasekhar's perturbation method.Many investigators have simulated quark stars or strange stars by accounting for anisotropic pressure [52–56]. Thirukkanesh et al. [57] investigated the feasibility of an anisotropic superdense star through the Vaidya-Tikekar ***metric for certain configurations of the anisotropy function. Panotopoulos et al. [58] derived an anisotropic solution for the interior of a relativistic star by considering that Newton's constant is a function of the radial coordinate. In the context of GR, Bhar et al. [59] examined a number of physical properties of the anisotropic solution for relativistic stars. Bhar [60] also examined interior solutions of anisotropic stars under the framework of $f(Q)$ gravity. Moreover, other anisotropic solutions were examined in several modified theories of gravity [61,62]. In this paper, we examine the influence of anisotropy on all physically relevant properties of the star to better understand its role in stellar structure within the context of $f(Q)$ gravity.

The paper is structured as follows: Sect. 2 outlines the mathematical formalism of $f(Q)$ gravity. Section 3 introduces a new class of solutions necessary for the viability of CSs. In Sect. 4, we examine the boundary conditions within $f(Q)$ gravity. Section 5 focuses on estimating the constant parameters for the stellar model. The physical behavior of anisotropic CSs, considering various aspects related to stellar data, is discussed in Sect. 6. Finally, Sect. 8 presents the concluding remarks on this work.

2 Mathematical formalism of $f(Q)$ gravity and the field equations

In our investigation of GR, we have identified the Levi-Civita affine connection as a critical element. This connection, when applied to the space-time manifold, ensures metric compatibility. By employing different manifolds and affine connections, it is possible to develop various interpretations of gravity [3,28]. Earlier research indicated that the Levi-Civita connection also uncovers two additional key geometric concepts: nonmetricity Q and torsion T. By relaxing these constraints, one can formulate numerous theories grounded in non-Riemannian geometry, where curvature, torsion, and nonmetricity all play pivotal roles. Within this framework, the $f(Q)$ gravity theory was developed, introducing a gravitational Lagrangian that incorporates an arbitrary function of nonmetricity, denoted as Q.

The extension of $f(Q)$ gravity plays a crucial role in understanding the universe's expansion. Jimenez et al. [28] were the pioneers in defining symmetric teleparallel gravity, now referred to as $f(Q)$ gravity. Building on the work of Zhao et al. [63] within the framework of $f(Q)$ gravity, we consider a general metric space-time where the metric tensor $g_{\mu\nu}$ and the connection $\Gamma^{\lambda}_{\mu\nu}$ are treated as independent variables. The nonmetricity of this connection is defined by the following equation,

$$Q_{\alpha\mu\nu} = \nabla_{\alpha} g_{\mu\nu} = \partial_{\alpha} g_{\mu\nu} - \Gamma^{\lambda}_{\alpha\mu} g_{\lambda\nu} - \Gamma^{\lambda}_{\alpha\nu} g_{\mu\lambda}. \tag{1}$$

By breaking down this affine connection into its independent components, we derive the following three components presented in a general manner

$$\Gamma^{\lambda}_{\mu\nu} = K^{\lambda}_{\mu\nu} + \{^{\lambda}_{\mu\nu}\} + L^{\lambda}_{\mu\nu},, \tag{2}$$

where $\{^{\lambda}_{\mu\nu}\}$ denotes Levi-Civita connection, $K^{\lambda}_{\mu\nu}$ is called contortion tensor, and $L^{\lambda}_{\mu\nu}$ defines disformation, the Levi-Civita connection ($\{^{\lambda}_{\mu\nu}\}$) is determined through the metric tensor $g_{\mu\nu}$ as:

$$\{^{\lambda}_{\mu\nu}\} \equiv \frac{1}{2} g^{\lambda\beta} (\partial_{\mu} g_{\beta\nu} + \partial_{\nu} g_{\beta\mu} - \partial_{\beta} g_{\mu\nu}). \tag{3}$$

However, $K^{\lambda}_{\mu\nu}$ is the contortion written as:

$$K^{\lambda}_{\mu\nu} \equiv \frac{1}{2} T^{\lambda}_{\mu\nu} + T_{(\mu\ \ \nu)}^{\ \ \lambda}. \tag{4}$$

The torsion tensor is defined as the skew-symmetric part of the affine connection, expressed as $T^{\lambda}_{\mu\nu} \equiv 2\Gamma^{\lambda}_{[\mu\nu]}$. Furthermore, the quantity $L^{\lambda}_{\mu\nu}$ is specified as:

$$L^{\lambda}_{\mu\nu} \equiv \frac{1}{2} Q^{\lambda}_{\mu\nu} - Q^{\lambda}_{(\mu\ \ \nu)}, \tag{5}$$

We now consider the nonmetricity conjugate as,

$$P^{\alpha}_{\mu\nu} = \frac{-1}{4} Q^{\alpha}_{\mu\nu} + \frac{1}{2} Q^{\alpha}_{(\mu\nu)} + \frac{1}{4} (Q^{\alpha} - \tilde{Q}^{\alpha}) g_{\mu\nu} - \frac{1}{4} \delta^{\alpha}_{(\nu} Q_{\mu)}. \tag{6}$$

The independent traces of the equations mentioned above are given as follows

$$Q_{\alpha} \equiv Q_{\alpha\mu}^{\ \ \mu} \qquad \tilde{Q}_{\alpha} \equiv Q^{\mu}_{\ \ \alpha\ \ \mu}. \tag{7}$$

The following is the definition of the nonmetricity scalar Q as:

$$Q = -Q_{\alpha\nu\mu} P^{\alpha\mu\nu}. \tag{8}$$

The $f(Q)$ gravity theory is characterized by the following action, which incorporates the use of Lagrange multipliers-

$$S = \int \sqrt{-g} d^4x \left[\frac{1}{2} f(Q) + \lambda^{\beta\mu\nu}_{\alpha} \mathcal{R}^{\alpha}_{\beta\mu\nu} + \lambda^{\mu\nu}_{\alpha} T^{\alpha}_{\mu\nu} + \mathcal{L}_m \right]. \tag{9}$$

In the previously stated equation, the determinant of the metric is denoted by g, while the Lagrangian density is represented by $\mathcal{L}_m$, with the Lagrange multipliers indicated as $\lambda^{\beta\mu\nu}_{\alpha}$.

The field equations have been derived from the action presented in Eq. (9) using the metric specified below:

$$\begin{aligned} T_{\mu\nu} = {} & \frac{2}{\sqrt{-g}} \nabla_{\alpha} (\sqrt{-g}\, f_Q P^{\alpha}_{\mu\nu}) \\ & + \frac{1}{2} g_{\mu\nu} f + f_Q (P_{\mu\alpha\beta} Q^{\alpha\beta}_{\nu} - 2 Q_{\alpha\beta\mu} P^{\alpha\beta}_{\nu}), \end{aligned} \tag{10}$$

where $f_Q \equiv \partial_Q f(Q)$ denotes the derivative of the function $f(Q)$ with respect to Q.

We employ the conventional notation for the energy-momentum tensor (EMT), as defined by,

$$T_{\mu\nu} \equiv \frac{2}{\sqrt{g}} \frac{\delta(\sqrt{-g}) \mathcal{L}_m)}{\delta g^{\mu\nu}}. \tag{11}$$

By differentiating Eq. (9) with regard to the affine connection, we get the result that follows,

$$\nabla_{\rho} \lambda_{\alpha}^{\ \ \nu\mu\rho} = \sqrt{-g} f_Q P^{\alpha}_{\mu\nu} + H_{\alpha}^{\ \ \mu\nu} - \lambda_{\alpha}^{\ \ \mu\nu}. \tag{12}$$

This density of hyper-momentum tensors may be expressed using the following formula:

$$H_{\alpha}{}^{\mu\nu} = \frac{-1}{2}\frac{\delta \mathcal{L}_m}{\delta T^{\alpha}_{\mu\nu}}. \tag{13}$$

We now simplify Eq. (12) to the following expression by taking into account the skew-symmetry property of μ and ν in the coefficients of the Lagrangian multipliers

$$\nabla_{\mu}\nabla_{\nu}(\sqrt{-g}f_Q P^{\mu\nu}_{\alpha} + H_{\alpha}{}^{\mu\nu}) = 0. \tag{14}$$

For $\nabla_{\mu}\nabla_{\nu}H_{\alpha}{}^{\mu\nu} = 0$, it gives

$$\nabla_{\mu}\nabla_{\nu}(\sqrt{-g}f_Q P^{\mu\nu}_{\alpha}) = 0. \tag{15}$$

In the absence of torsion and curvature, the affine connection is represented as follows,

$$\Gamma^{\alpha}_{\mu\nu} = \left(\frac{\partial x^a}{\partial \xi^{\lambda}}\right)\partial_{\mu}\partial\nu\xi^{\lambda}. \tag{16}$$

In the context of a particular coordinate system, commonly referred to as a coincident gauge where $\Gamma^{\alpha}_{\mu\nu} = 0$, the nonmetricity simplifies to

$$Q_{\alpha\mu\nu} = \partial_{\alpha}g_{\mu\nu}. \tag{17}$$

By employing this coordinate system, computational complexity is minimized, as the metric becomes the sole fundamental variable. However, maintaining diffeomorphism invariance in the action is only guaranteed for STGR. To overcome this issue, we utilize the covariant formulation of $f(Q)$ gravity. The relationship specified in Eq. (16) is inertial, requiring the affine connection to be determined in the absence of gravity [22]. Nonetheless, the off-diagonal element of the field equations in the coincident gauge puts substantial restrictions on $f(Q)$ gravity, resulting in the formulation of intricate functional expressions for $f(Q)$.

We consider the general static and SS spacetime metric within stellar systems' interiors.

$$ds^2_{-} = -X^2(r)dt^2 + Y^2(r)dr^2 + r^2(d\theta^2 + \sin^2\theta\, d\phi^2). \tag{18}$$

where the coordinate $x^i_{-} = (t, r, \theta, \phi)$, $i = 0, 1, 2, 3$, X and Y are metric potentials. By putting Eq. (18) into Eq. (8), we get an additional equation, expressing the nonmetricity scalar Q as,

$$Q(r) = -\frac{2}{r}\frac{1}{Y^2}\left(2\frac{X'}{X} + \frac{1}{r}\right). \tag{19}$$

In this context, the prime ($'$) denotes the derivative with respect to r. The energy-momentum tensor for an anisotropic fluid in a SS system is expressed as follows,

$$T_{\mu\nu} = (\rho + p_t)u_{\mu}u_{\nu} + p_t g_{\mu\nu} + (p_r - p_t)\eta_{\mu}\eta_{\nu}. \tag{20}$$

Here, the four-velocity is represented by u_{μ}, and η_{μ} indicates the unit space-like vector directed radially, which satisfies the conditions $u^{\mu}u_{\mu} = -1$, $\eta^{\mu}\eta_{\mu} = 1$, and $u^{\mu}\eta_{\nu} = 0$. Furthermore, $\rho(r)$ denotes the energy density, $p_r(r)$ represents the radial pressure, and $p_t(r)$ is the tangential pressure.

The constituent component of the field's equations (10) governing the behavior of anisotropic fluid (20) are expressed as follows.

$$\rho = -\frac{1}{r^2Y^2} + \left[rQ' f_{QQ}(Y^2-1) + f_Q \times \left((Y^2-1)\left(1 + r\frac{X'}{X}\right) + r(1+Y^2)\frac{Y'}{Y}\right) + \frac{1}{2}r^2 f Y^2\right], \tag{21}$$

$$p_r = -\frac{1}{r^2Y^2}\left[rQ' f_{QQ}(Y^2-1) + f_Q\left((Y^2-1) \times \left(1 + r\frac{X'}{X} + r\frac{Y'}{Y}\right) - 2r\frac{X'}{X}\right) + \frac{1}{2}f r^2 Y^2\right], \tag{22}$$

$$p_t = -\frac{1}{rY^2}\left[-rQ' f_{QQ}\frac{X'}{X} + f_Q\left((Y^2-2)\frac{X'}{X} - r\frac{X'^2}{X^2} + \frac{Y'}{Y}\left(Y^2 + r\frac{X'}{X}\right) - r\left(\frac{X''}{X} - \frac{X'^2}{X^2}\right)\right) + \frac{1}{2}rfY^2\right], \tag{23}$$

$$\frac{\cot\theta}{2}Q' f_{QQ} = 0, \tag{24}$$

where $f_Q = \frac{df}{dQ}$, $f_{QQ} = \frac{d^2f}{dQ^2}$.

3 A new class of solution in $f(Q)$ gravity

Assuming the affine connection vanishes in the chosen coordinate system, $f(Q)$ gravity requires vacuum solutions, i.e., $T_{\mu\nu} = 0$. This leads to the derivation of the off-diagonal component of the field equation (24). By combining Eq. (10) with Eq. (24), we obtain $f_{QQ} = 0$, indicating that the function $f(Q)$ must be linear. Nonlinear choices for $f(Q)$, such as $f(Q) = Q^2$, result in inconsistencies within the Einstein field equations (EFEs) and their solutions. Therefore, nonlinear forms of $f(Q)$ gravity do not produce consistent equations of motion. If nonlinear $f(Q)$ gravity is to be studied, a more generalized form of the SS metric within the coincident gauge is required. For a detailed discussion, see Zhao's work [63]. In this study, we consider a linear function by setting f_{QQ} to zero and aligning the SS coordinate system (18) with an affine connection where $\Gamma^{\mu}_{\epsilon\nu}$ equals zero.

In order to accurately describe a realistic compact stellar model, it is crucial to identify an appropriate function, denoted as $f(Q)$. Wang et al. [4] highlighted the importance of selecting a function whose second derivative with respect to Q, f_{QQ}, equals zero, ensuring compatibility between the solution for the compact star and the Schwarzschild (Anti-) de Sitter solution at the outer boundary. As a result, to investigate physically plausible stellar models, we choose a linear function $f(Q)$, given by

$$f(Q) = \alpha Q + \beta, \tag{25}$$

where α and β are arbitrarily treated as model parameters. For the choice of $\alpha = 1, \beta = 0$, one can recover the case of classical GR.

Using Eq. (25) into the Eqs. (21)–(24), the field equations are obtained in view of $f(Q)$ gravity as,

$$\rho = \frac{1}{r^2}\left[\alpha + \frac{\alpha}{Y^2}\left(2r\frac{Y'}{Y} - 1\right) - \frac{1}{2}r^2\beta\right], \tag{26}$$

$$p_r = \frac{1}{r^2}\left[-\alpha + \frac{\alpha}{Y^2}\left(2r\frac{X'}{X} + 1\right) + \frac{1}{2}r^2\beta\right], \tag{27}$$

$$p_t = \frac{Y^{-2}}{r}\left[\frac{1}{2}\beta r Y^2 + \alpha\left(1 + r\frac{X'}{X}\right)\left(\frac{X'}{X} - \frac{Y'}{Y}\right) + \alpha r\left(\frac{X''}{X} - \frac{X'^2}{X^2}\right)\right]. \tag{28}$$

Within the physics literature, anisotropic pressure characterizes the directional diversity in fluid dispersion. However, under certain plausible circumstances, pressure anisotropy can be represented by $\Delta = (p_t - p_r)$, signifying the progressive behavior of the stellar object. By employing Eqs. (27)–(28), the pressure anisotropy in our static configuration system is examined

$$\Delta = \frac{X^{-2}Y^{-2}}{r^2}\left[-\alpha r^2(1+Y^2)X'^2 + X^2\left(\alpha + (-\alpha + \beta r^2)Y^2 + \alpha r Y Y'\right) + \alpha r X\left(X'(2 - Y^2 + rYY') + rX''\right)\right]. \tag{29}$$

The mass $m(r)$ enclosed within a radius r of the stellar object is defined as

$$m(r) = \frac{1}{2}\int_0^r x\rho(x)dx. \tag{30}$$

Given that the system of equations (26)–(28) involves five unknowns, namely ρ, p_r, p_t, X, Y, it necessitates the incorporation of two supplementary constraint relations to achieve complete solutions.

For a stellar model to be physically valid, it is imperative that the metric potentials $(g_{\mu\nu})$ exhibit regularity at the central point $(r = 0)$.

In a recent study by Das et al. [64], a novel analytical stellar model within the framework of GR was examined, offering insights into various attributes of observed pulsars. Building upon this premise, in this work we investigate the form of the metric potential g_{rr} as follows-

$$Y^2(r) = \left(Ar^4 - Br^2 + 1\right)^{-1}, \tag{31}$$

here A and B represent model parameters referred to as curvature constraints, with dimensions of $(length)^{-4}$ and $(length)^{-2}$, respectively.

Taking use of Eq. (31) into Eq. (29) and rearranging, one obtains

$$\frac{X''}{X} + \frac{(Ar^4 - 1)}{r(1 - Br^2 + Ar^4)}\frac{X'}{X} = \frac{8\pi\Delta - \alpha Ar^2}{(1 - Br^2 + Ar^4)}. \tag{32}$$

Considering Eq. (32) as a differential equation in X, its solvability hinges on knowledge of $\Delta(r)$ form. To render the equation integrable, we postulate a quadratic form of anisotropy, thereby facilitating its solution,

$$\Delta(r) = \alpha Ar^2. \tag{33}$$

This quadratic form of anisotropy is both physically plausible and diminishes at the central point of the star ($r = 0$). Herrera and Santosh [45] demonstrated that such anisotropy could emerge in CSs as a consequence of slow rotation. Furthermore, this selection offers a closed-form solution for Eq. (32),

In view of Eq. (33), the Eq. (32) provide

$$\frac{X''}{X} + \frac{(Ar^4 - 1)}{r(1 - Br^2 + Ar^4)}\frac{X'}{X} = 0, \tag{34}$$

which gives after-integration

$$X(r) = k_2 + \frac{k_1}{2\sqrt{A}}\log\left[2Ar^2 - B + 2\sqrt{A(1 - Br^2 + Ar^4)}\right], \tag{35}$$

where k_1, k_2 are integrating constants which further can be determined by using the boundary conditions.

After inserting the value of $X(r)$ and $Y(r)$ into field equations (26)–(28), one obtain

$$\rho(r) = 3\alpha B - 5\alpha Ar^2 - \frac{\beta}{2}, \tag{36}$$

$$p_r(r) = \alpha\left(\frac{4k_1\sqrt{A\left(Ar^4 - Br^2 + 1\right)}}{k_1\log\left(2\sqrt{A\left(Ar^4 - Br^2 + 1\right)} + 2Ar^2 - B\right) + 2\sqrt{A}k_2} + Ar^2 - B\right) + \frac{\beta}{2}, \tag{37}$$

$$p_t(r) = \frac{\alpha}{\sqrt{A\left(Ar^4 - Br^2 + 1\right)}\left(k_1\log\left(2\sqrt{A\left(Ar^4 - Br^2 + 1\right)} + 2Ar^2 - B\right) + 2\sqrt{A}k_2\right)} \times\left[4A^{3/2}k_2r^2\sqrt{A\left(Ar^4 - Br^2 + 1\right)} + 4A^2k_1r^4 - 4Ak_1\left(Br^2 - 1\right) + k_1\left(2Ar^2 - B\right)\right. \left.\times\sqrt{A\left(Ar^4 - Br^2 + 1\right)}\log\left(2\sqrt{A\left(Ar^4 - Br^2 + 1\right)} + 2Ar^2 - B\right) - 2\sqrt{A}Bk_2\sqrt{A\left(Ar^4 - Br^2 + 1\right)}\right] + \frac{\beta}{2}. \tag{38}$$

4 Boundary conditions in $f(Q)$ gravity

In this section, we examine the appropriate boundary conditions required for solving the Einstein field equations (EFEs) within the framework of $f(Q)$ gravity. This involves ensuring compatibility between solutions in the interior and exterior regions of space-time. According to the generalized Jabsen–Birkhoff theorem, the solution to the EFEs in the case of empty space-time describing the gravitational field around an object in the presence of a cosmological constant $\wedge$-corresponds to the Schwarzschild (Anti-) de Sitter metric. When considering stellar systems within the context of $f(Q)$ gravity, the exterior space-time is generally described by the Schwarzschild (Anti-) de Sitter geometry [4]. The expression for the Schwarzschild (Anti-) de Sitter metric is given as follows:

$$ds_+^2 = -\left(1 - \frac{2M}{\mathbf{r}} - \frac{\wedge}{3}\mathbf{r}^2\right)dt^2 + \frac{d\mathbf{r}^2}{\left(1 - \frac{2M}{\mathbf{r}} - \frac{\wedge}{3}\mathbf{r}^2\right)} + \mathbf{r}^2\left(d\theta^2 + \sin^2\theta\, d\phi^2\right) \quad (39)$$

where exterior coordinate is $x_+^{\mu} = (T, \mathbf{r}, \theta, \phi)$.

M describes the mass of the stellar object (also known as Schwazschild mass) and $\wedge$ is a cosmological constant. It's worth highlighting that the cosmological constant, denoted by $\wedge$, is contingent upon the constants α and β, expressed as $\wedge = \frac{\beta}{2\alpha}$. For the mathematical framework to be significantly influenced, the cosmological constant must be substantially high. However, in this context, the empirical support is minimal, resulting in the insignificance of $\wedge$ in affecting the current stellar model. Based on available numerical data, the cosmological constant $\wedge$ approximates $10^{-46}/km^2$, but such value has no relevance in the present investigation.

We examine the smooth connection between the interior space-time metric ds_-^2 (represented by Eq. (18)) and the exterior metric ds_+^2 across the hypersurface $\Sigma : r = R$. This boundary, denoted as Σ, acts as the division between the interior and exterior regions of the SS stellar system. Employing the Darmois–Israel methodology [65,66], we recognize that in the framework of f(Q) gravity, additional constraints must be satisfied due to the presence of non-metric connections, ensuring the feasibility of such matching configurations.

(i) The continuity of the first fundamental form (the metric) at boundary $\Sigma : r = R$ that is

$$g_{tt}^- \overset{\Sigma}{=} g_{TT}^+, \quad g_{rr}^- \overset{\Sigma}{=} g_{\mathbf{rr}}^+,$$

which provide us

$$X^2(R) = \left(1 - \frac{2M}{R} - \frac{\wedge}{3}R^2\right) \quad (40)$$

$$Y^2(R) = \left(1 - \frac{2M}{r} - \frac{\wedge}{3}r^2\right)^{-1}. \quad (41)$$

(ii) The continuity of the second fundamental form (the extrinsic curvature) at the boundary $\Sigma : r = R$ gives [67]

$$p_r(R) = 0 \implies \frac{\alpha\left(X + 2RX'\right)}{XY^2R^2} + \frac{1}{2}\beta = \frac{\alpha}{R^2}, \quad (42)$$

Therefore, Eqs. (40)–(42) serve as essential boundary conditions f(Q) gravity. In the context of stellar modeling, these boundary conditions play a crucial role in determining the numerical values of arbitrary constant parameters. Consequently, we can deduce the model parameters in our study through the utilization of these boundary conditions.

5 Estimation of model parameters and relevant with astrophysical stellar data

In this section, we discuss the estimation of arbitrary parameters- model parameters k_1, k_2 alongside the total mass M utilizing the boundary as mentioned earlier conditions.

Using Eqs. (31), (32) and (37) into boundary conditions (40), (41) and (42), the value of k_1, k_2 and M are stated as,

$$k_1 = \frac{\sqrt{A}\sqrt{AR^4 - BR^2 + 1}\left(2\alpha\left(B - AR^2\right) - \beta\right)}{4\alpha\sqrt{A\left(AR^4 - BR^2 + 1\right)}}, \quad (43)$$

$$k_2 = \frac{\sqrt{AR^4 - BR^2 + 1}}{8\alpha\sqrt{A\left(AR^4 - BR^2 + 1\right)}} \times\Bigg[2\alpha\left(4\sqrt{A\left(AR^4 - BR^2 + 1\right)} + \left(AR^2 - B\right) \times \log\left(2\sqrt{A\left(AR^4 - BR^2 + 1\right)} + 2AR^2 - B\right)\right) + \beta\log\left(2\sqrt{A\left(AR^4 - BR^2 + 1\right)} + 2AR^2 - B\right)\Bigg], \quad (44)$$

$$M = \frac{R^3\left[6\alpha\left(B - AR^2\right) - \beta\right]}{12\alpha}. \quad (45)$$

We conducted an analysis of astrophysical data pertaining to compact star Vela $X-1$. Utilizing Eqs. (43) and (44), we determined the numerical values of constant parameters k_1 and k_2 for the CSs using the provided astrophysical data points, as elaborated in Table 1. These parameters were subsequently employed in tandem with the astrophysical data to compute quantities such as ρ, p_r, p_t, Δ, mass (M), and red-shift (z), which were then visually represented to elucidate their trends. Throughout this study, the values of β is assumed to be 0.0001 respectively.

Table 1 The values of central density (ρ_c), surface density (ρ_s), central pressure (p_c), surface red-shift (z_s), adiabatic index (Γ), k_1 and k_2

α	ρ_c (gm/cm^3)	ρ_s (gm/cm^3)	p_c (dyne/cm^2)	Γ	z_s	k_1	k_2
1.0	4.48395 x 10^{14}	3.58617×10^{14}	4.62499×10^{34}	6.44387	0.304341	0.00120782	5.12187
1.25	5.61165×10^{14}	4.49289×10^{14}	5.80236×10^{34}	6.47239	0.30312	0.00121333	5.14289
1.5	6.73935×10^{14}	5.39892×10^{14}	6.9851×10^{34}	6.48926	0.302511	0.00121692	5.15641
1.75	7.86705×10^{14}	6.30564×10^{14}	8.16225×10^{34}	6.50322	0.301903	0.00121956	5.16649
2.0	8.99475×10^{14}	7.22133×10^{14}	9.26746×10^{34}	6.53534	0.299482	0.00122238	5.17889

6 Physical viability of the anisotropic stellar model

6.1 Regularity of the metric potentials

In order for the stellar model to behave appropriately, it is necessary for the metric potential to remain finite and smooth at the central point of the star. In our analysis, we demonstrate that at the center ($r = 0$), the metric potential g_{rr} conforms to these criteria as indicated by $Y^2(r = 0) = 1$. Furthermore, we have derived the expression for the potential $g_{tt} = X^2(r)$ (refer to Eq. (35)), which elucidates that $X^2(r = 0)$ equates to a constant value. Specifically, it is expressed as $k_2 + \frac{1}{2\sqrt{A}} k_1 \log\left(2\sqrt{A} - B\right)$, indicating its regularity at the center. This is visually corroborated by Fig. 1, where the metric potentials exhibit positivity, finiteness, smoothness, and a monotonically increasing behavior within the confines of the star for different values of α.

6.2 Qualitative analysis of the physical parameters: density, pressures, and anisotropy

In order to establish a physically viable stellar model, it is imperative that both density and pressure exhibit finiteness and a decreasing trend within the star. At the boundary $r = R$, the radial pressure diminishes to zero, while the tangential pressure maintains positivity across the stellar structure, as delineated in Figs. 2 and 3. Additionally, it is observed that the central density of the star, denoted as ρ_c, adheres to the condition of being finite and non-negative, characterized by $\rho_c = 3\alpha A - \frac{1}{2}\beta$. This behavior underscores a progressive increase in density towards the core, peaking at $r = 0$, signifying greater compactness in the core compared to the outer layers. Notably, both pressures exhibit minima in proximity to the boundary $r = R$, with a subsequent rise towards the center at $r = 0$. Consequently, the hydrostatic force engendered by these pressures is ascertained to be positive, exerting an outward influence. Furthermore, the central values of density and pressures both are increasing when α increases.

A stable and physically sustainable celestial body necessitates a hydrostatic force feature that counteracts gravitational attraction, thereby averting gravitational collapse a fundamental criterion. Moreover, the anisotropy of such a celestial body is influenced by two opposing forces: a repulsive force when $\Delta > 0$ and an attractive force when $\Delta < 0$. The repulsive force acts to disperse the fluid from the body, while the attractive force draws it inward. Under isotropic conditions ($p_r = p_t$), these forces balance each other, resulting in a state of equilibrium, mathematically denoted as $\Delta = 0$. However, moving away from the stellar core, the anisotropy experiences a positive increase. This augmentation occurs because the repulsive force gains dominance with increasing distance from the star, as depicted in Fig. 3. The anisotropy graph is expected to exhibit a consistent positive increment in the vicinity of the star. On the other hand, it is seen that the magnitude of anisotropy increases when α increases. Consequently, the preceding examination of physical parameters clarifies the notable characteristics of CSs inside the context of $f(Q)$ gravity.

6.3 Energy conditions

This section delves into the physical attributes of our stellar models, delving into various energy conditions (EC). EC plays a pivotal role in assessing the stability of the stellar model. Positive energy bounds delineate the authentic and physical attributes of anisotropic matter. A stellar structure is deemed physically tenable when it upholds specific EC throughout its evolution. Leveraging the gravitational theory framework enables us to articulate energy criteria as local inequalities governing the interaction between energy density (ρ) and pressures (p_r, p_t), under certain constraints. The positivity of density and pressures implies that the null energy condition (NEC), weak energy condition (WEC), and strong energy condition (SEC) are indeed positive. The dominant energy condition (DEC) is employed to scrutinize the stability of a compact star.

The mathematical expression of such constraints is as follows-

$$\text{NEC:} \quad \rho + p_r \geq 0, \rho + p_t \geq 0, \tag{46}$$

$$\text{WEC:} \quad \rho \geq 0, \rho + p_r \geq 0, \rho + p_t \geq 0, \tag{47}$$

$$\text{SEC:} \quad \rho + p_r + 2p_t \geq 0, \tag{48}$$

$$\text{DEC:} \quad \rho \geq 0, \rho - p_r \geq 0, \rho - p_t \geq 0. \tag{49}$$

$$\text{TEC:} \quad \rho - p_r - 2p_t \geq 0. \tag{50}$$

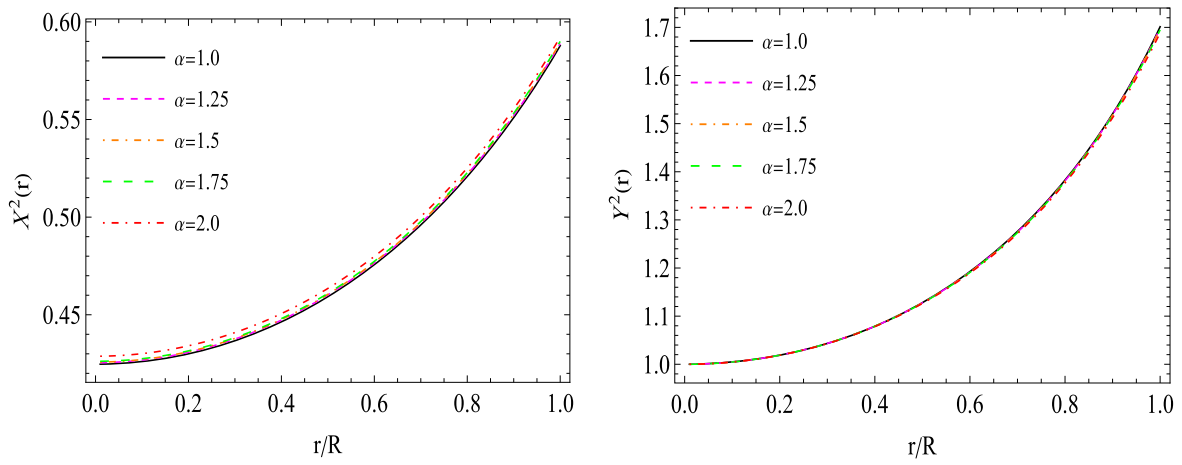

Fig. 1 The variation of metric potentials $X^2(r)$ and $Y^2(r)$ versus radius r/R within CSs. The numerical values of the parameters $A = 0.000002\ \text{km}^{-4}$, $B = 0.0028\ \text{km}^{-2}$, and $\beta = 0.001$ are taken to plot the figures

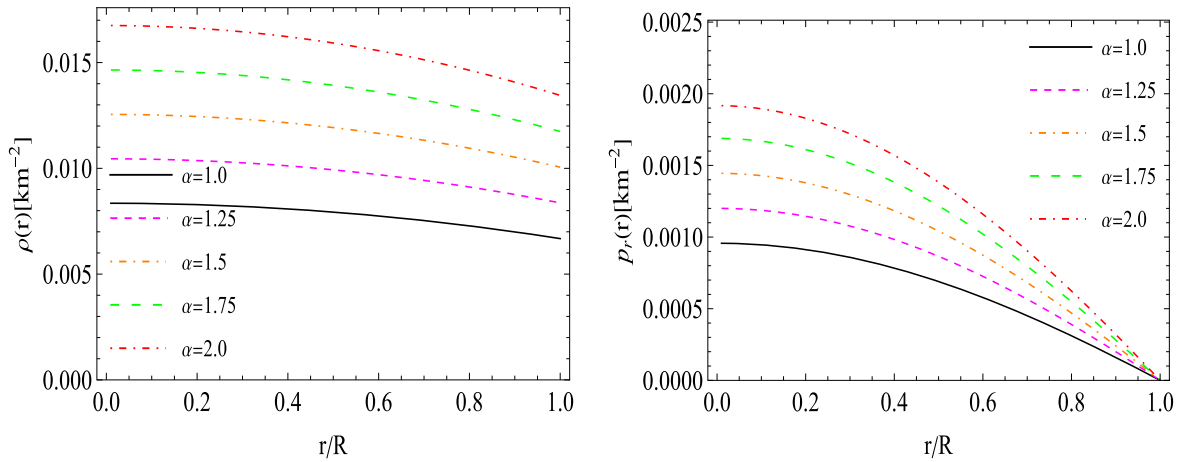

Fig. 2 The behavior of density ρ - (left panel) and radial pressure p_r - (right panel) within compact stars with same values as employed in Fig. 1

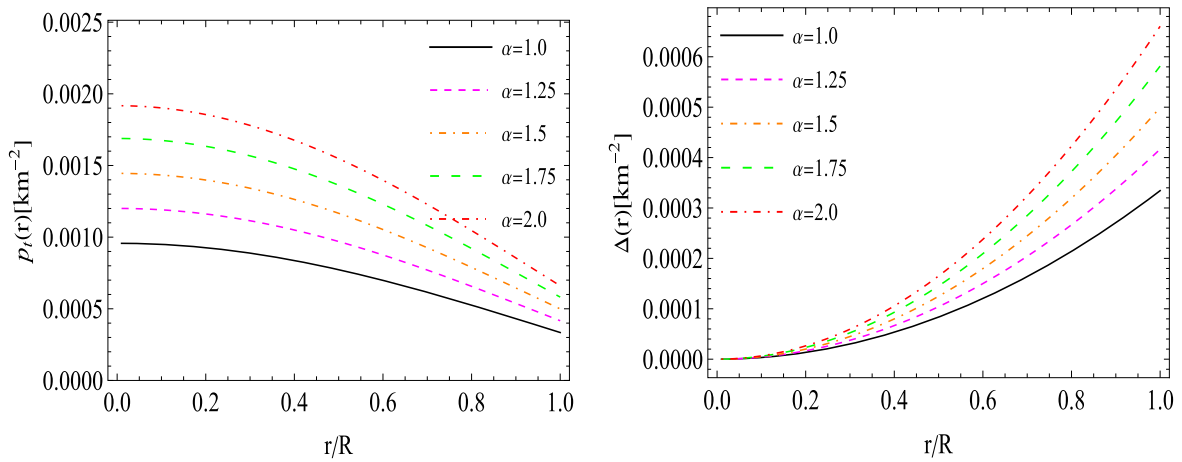

Fig. 3 The behavior of tangential pressure p_t - (left panel) and anisotropy Δ- (right panel) within compact stars with same values as employed in Fig. 1

Given that both pressure and density are positive throughout the star configuration, our derived solution inherently satisfies the DEC, WEC, and SEC. We only need to validate the DEC and TEC with the celestial object. Figure 4 demonstrates that the energy criteria DEC and TEC are fulfilled throughout the star, indicating a stable and well-behaved model.

6.4 EoS parameters

The equation of state (EoS) characterizes the ratio of energy density and pressures inside the stellar configuration, represented as

$$\omega_r = \frac{p_r}{\rho}, \qquad \omega_t = \frac{p_t}{\rho}. \tag{51}$$

It provides significant insights into the composition of the star's constituent matter. To elucidate the distribution of ordinary matter, it is imperative for the equation of state (EoS) parameter to remain below 1, represented as $0 < \omega_r < 1$ and $0 < \omega_t < 1$ for all taken values of $f(Q)$ parameter α. Figure 5 illustrates the radial and transverse fluctuations of the EoS parameters ω_r and ω_t, revealing that they consistently reside within the 0 to 1 range throughout the star's interior. These findings suggest a strong alignment between the observed EoS parameter variations and our proposed stellar models.

6.5 Tolman–Oppenheimer–Volkoff (TOV) equation: equilibrium condition

In this subsection, we investigated the equilibrium stability of the stellar model within the framework of f(Q) gravity, considering the gravitational force, hydrostatic force, and anisotropic force. The internal structure of anisotropic CS is described by the TOV equation, which was introduced in the pioneering works by Tolman, Oppenheimer, and Volkoff [68,69].

According to the TOV equation, the equilibrium condition for these forces may be formulated in the following manner,

$$M_G \frac{\rho + p_r}{r^2}\frac{Y}{X} + \frac{dp_r}{dr} - \frac{2}{r}\Delta = 0, \tag{52}$$

where M_G represents the effective gravitational mass, which is calculated from the Tolman–Whittaker mass equation expressed as,

$$M_G = \frac{X'}{X}\frac{r^2 X}{Y}. \tag{53}$$

By using the equation for M_G in Eq. (52), we get

$$\frac{X'}{X}(\rho + p_r) + \frac{dp_r}{dr} - \frac{2}{r}\Delta = 0. \tag{54}$$

The TOV equation satisfies the equilibrium condition $F_g + F_h + F_a = 0$, signifying that the cumulative forces inside the star system need to equal to zero, where

$$\text{Gravitational force: } F_g = -\frac{X'}{X}(\rho + p_r), \tag{55}$$

$$\text{Hydrostatic force: } F_h = -\frac{dp_r}{dr}, \tag{56}$$

$$\text{Anisotropic force: } F_a = \frac{2}{r}\Delta = \frac{2}{r}(p_t - p_r). \tag{57}$$

The data depicted in Fig. 6 indicate that every force satisfies the necessary conditions for maintaining the equilibrium stability of the stellar system.

6.6 Stability criteria via cracking concept

Another approach to exploring the potential enduring anisotropic structure of a compact stellar object involves investigating the occurrence of overturning or fracturing within a model. By assessing the possibility of cracking or overturning, it becomes feasible to evaluate the potential stability of the star. As fluid elements within the compact star undergo acceleration, there arises a propensity for the star to fracture at a specific juncture, assuming the star experiences neither compression nor expansion. This fracture susceptibility termed the stability condition of the star, was proposed by Herrera [70] and utilized in a study to ascertain the stability of CS models. According to this approach, the speed of sound with CS models must follow causality constraints in order to be considered physically acceptable; and radial velocity (v_r^2) must be greater than the tangential velocity (v_t^2). The formula for v_r^2 and v_t^2 are given as follows:

$$v_r^2 = \left|\frac{dp_r}{d\rho}\right|, \quad v_t^2 = \left|\frac{dp_t}{d\rho}\right|. \tag{58}$$

respectively. To assess the resilience of our proposed model, we investigated the parameters $0 < v_r^2 < 1$ and $0 < v_t^2 < 1$ within celestial bodies, assuming a speed of light c equal to 1. Figure 7 provides visual evidence supporting the potential stability and adherence to causality conditions of the analyzed $f(Q)$ gravity models. Furthermore, to evaluate the stability of anisotropic compact structures in order to analyze Herrera's cracking notion about the stability of compact objects. The investigation indicates that a model is theoretically stable if it meets the condition $0 \leq v_r^2 - v_t^2 > 0$, provided there is no sign change of $v_r^2 - v_t^2$ inside the star's radius. Since the requirement $0 \leq v_0^2 - v_t^2 > 0$ is fulfilled by our model because v_r^2 always greater than v_t^2 throughout the star for all values of α, we may conclude that the model adheres to Herrera's cracking concept.

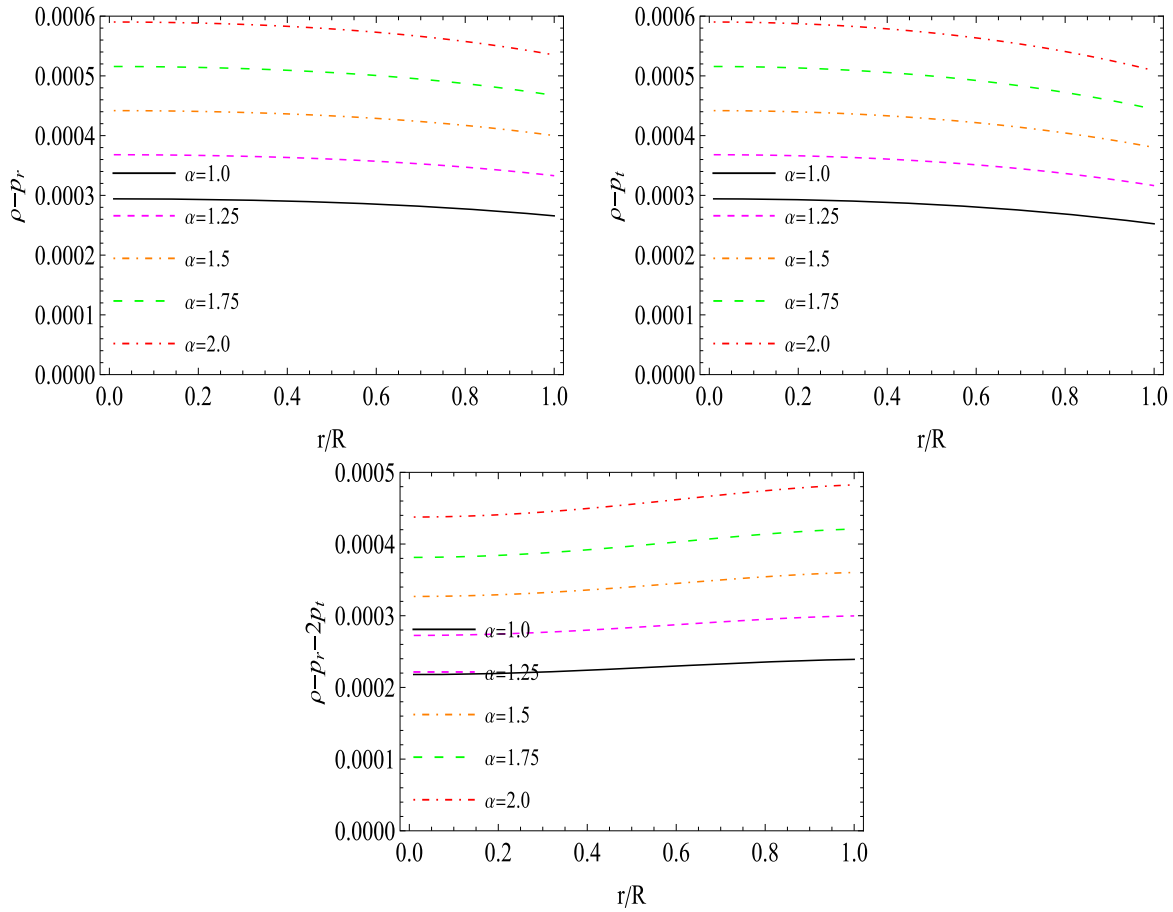

Fig. 4 The nature of energy conditions: the variation of $\rho - p_r$ -(upper left panel), $\rho - p_t$ -(upper right panel), $\rho - p_r - 2p_t$ -(bottom panel) within compact star

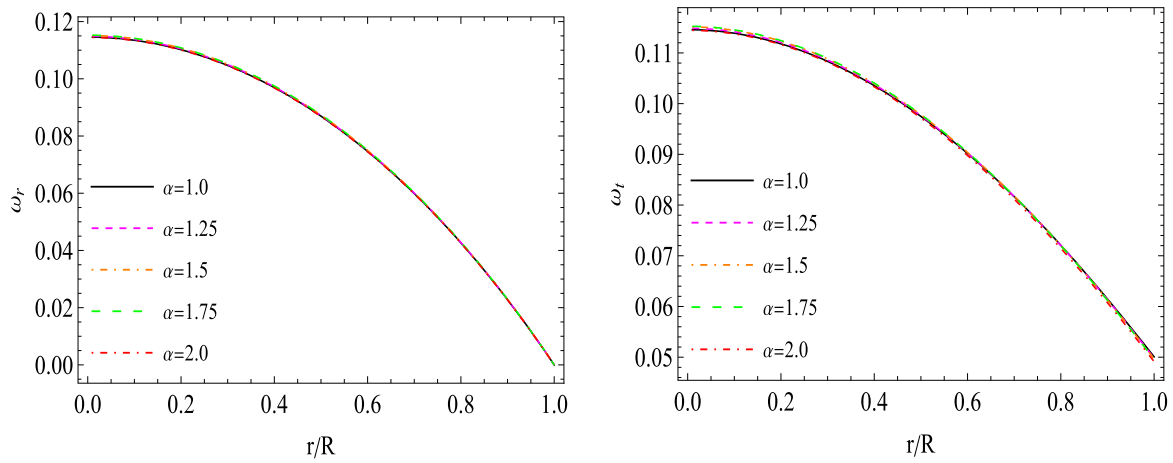

Fig. 5 The behavior of EoS parameters ω_r and ω_t within compact stars for the parameter values $A = 0.000002$ km^{-4}, $B = 0.0028$ km^{-2}, and $\beta = 0.001$

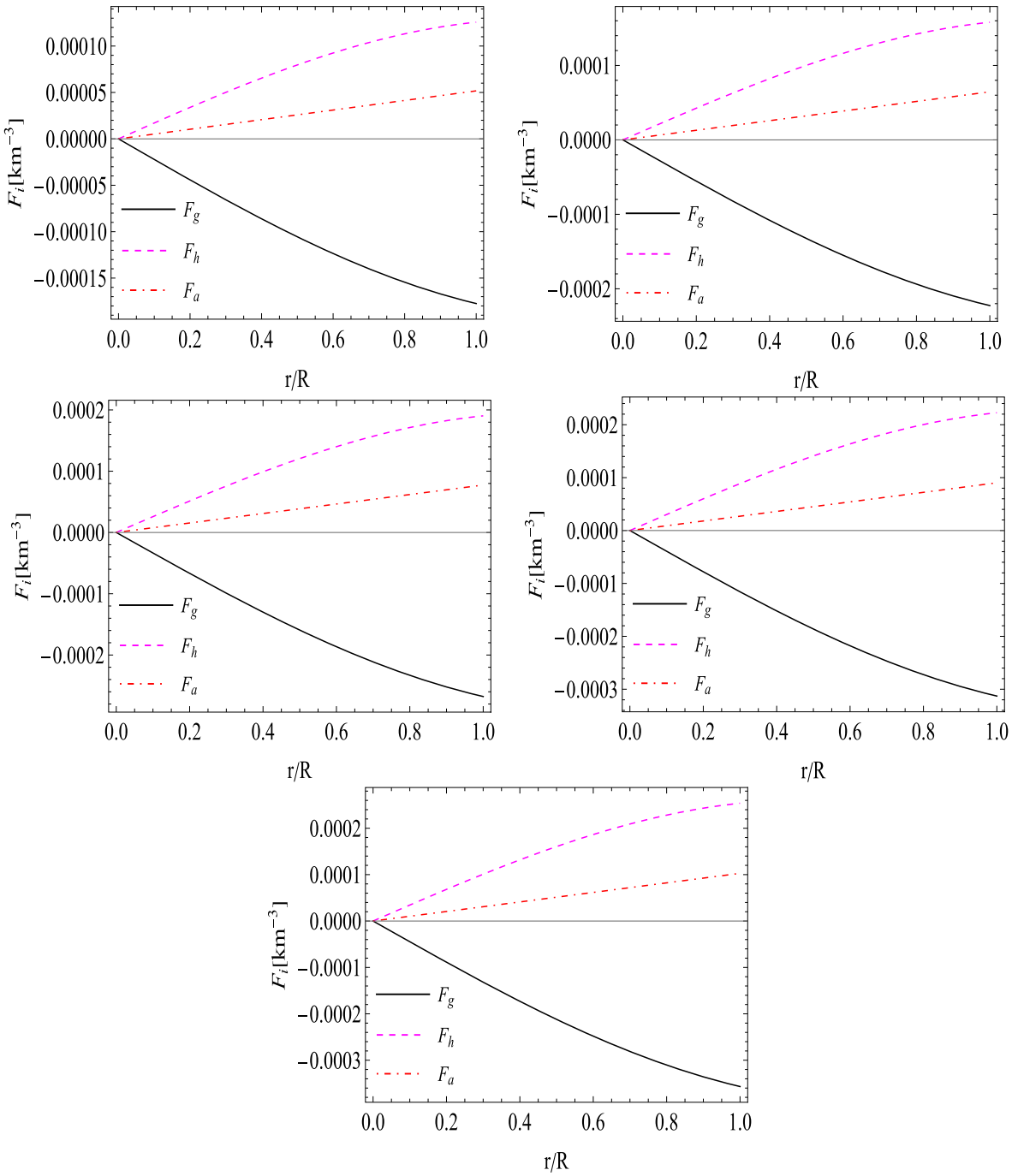

Fig. 6 The equilibrium condition: Figures showing the nature of different forces (F_i : F_g, F_g, F_h) within the compact stars, for $\alpha = 1.0$ - (upper left panel), for $\alpha = 1.25$ (upper right panel), for $\alpha = 1.50$ (middle left panel), for $\alpha = 1.75$ (middle right panel) and $\alpha = 2.0$ (lower panel) for similar values as used in Fig. 5

6.7 Adiabatic index

For a stable stellar configuration, a comprehensive analysis of the adiabatic index (Γ) and a careful examination of the instability criteria for anisotropic stellar models are essential. Stability considerations are critical when analyzing both Newtonian and relativistic fluid models for compact objects. In Newtonian frameworks, the average adiabatic index must satisfy $\Gamma_r > \frac{4}{3}$ to ensure stability. Knutsen [73] demonstrated mathematically that for isotropic fluid models, the adiabatic index exceeds unity when the pressure-to-energy density ratio decreases monotonically with radial distance, signifying a decrease in temperature outward from the center. Building on this, Herrera et al. [70,74,75] formulated

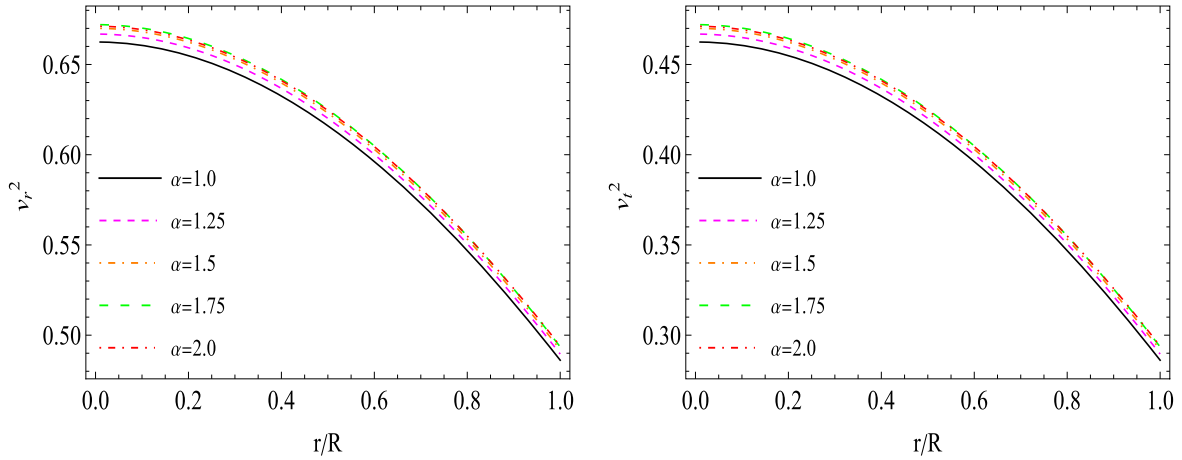

Fig. 7 The stability criteria: variation of sound's radial velocity v_r^2 - (left panel) and tangential velocity v_t^2 - (right panel) within compact stars

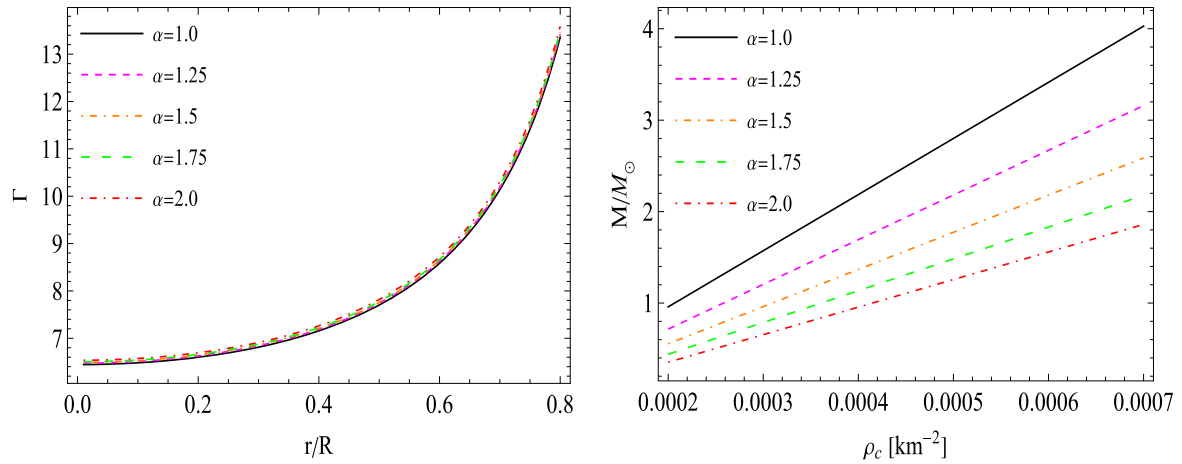

Fig. 8 The stability criteria: variation of adiabatic index Γ (left panel) versus fractional radius r/R and mass $M/M_\odot$ versus central density ρ_c within compact stars

criteria for assessing the stability of relativistic anisotropic stars.

The adiabatic index is defined as follows

$$\Gamma = \frac{\rho + p_r}{p_r}\frac{dp_r}{d\rho}, \tag{59}$$

The findings demonstrate that the values of Γ constantly exceed $\frac{4}{3}$ over the whole stellar interior, as seen in Fig. 8 (left panel) and Table 1. Therefore, our model is stable.

6.8 Harrison–Zeldovich–Novikov criterion

We use the Harrison–Zeldovich–Novikov (HZN) criteria [71, 72] to evaluate stability. The resultant inequality is used to evaluate the HZN stability criteria,

- $\frac{dM}{d\rho_c} > 0$ → stable stellar structure
- $\frac{dM}{d\rho_c} < 0$ → unstable stellar structure.

This implies that the total mass (M) should be increasing with central density ρ_c. Therefore, we derive the subsequent procedures to validate the aforementioned condition for the obtained solution,

$$M = -\frac{R^3\left(8\pi\rho_c - 3A\alpha R^2 - \beta\right)}{6\alpha}, \tag{60}$$

$$\frac{dM}{d\rho_c} = \frac{4\pi R^3}{3\alpha}. \tag{61}$$

The aforementioned formula shows that $\frac{dM}{d\rho_c}$ cannot be negative for positive values of α. The overall mass is a monotonically rising function of central density. Consequently, the current model establishes a stable star configuration in accordance with the HZN stability criterion. Figure 8 (right panels) demonstrates that $M(\rho_c)$ is a monotonically rising function of ρ_c, exhibiting positive behavior across the system.

6.9 Red-shift analysis

We have conducted an analysis of the redshift observed in CSs. The phenomenon of gravitational redshift occurs when electromagnetic waves, or photons, emanate from a gravitational object and seemingly lose energy. It is noteworthy that according to GR theory, which elucidates the relationship between gravitational fields, spacetime, and matter, this redshift effect is predicted. Since photons travel at a constant speed, their apparent energy loss is manifested as a change in frequency rather than velocity. Consequently, the wavelength of the photon increases while the frequency of the wave decreases due to this energy loss. Observations in various astrophysical scenarios, such as those near black holes or within the vicinity of massive galaxies, have documented this phenomenon. Gravitational redshift stands as a fundamental aspect of modern physics, subject to extensive research and empirical investigation.

For maintaining stability within a SS anisotropic compact star, it is imperative that the inner redshift increases towards the center and decreases towards the boundary at $r = R$. The formula representing the gravitational redshift within the CS is articulated as follows:

$$z(r) = \frac{1}{X} - 1 = \frac{2\sqrt{A}}{k_1 \log\left(2\sqrt{A\left(Ar^4 - Br^2 + 1\right)} + 2Ar^2 - B\right) + 2\sqrt{A}k_2} - 1 \tag{62}$$

Figure 9 depicts the profile of gravitational red-shift variation, demonstrating a decreasing nature from the core region to the outer boundary surface of a compact star.

The work of Ivanov [76] delineates the criteria governing the surface red-shift ($z_s = z(r = R)$) within an anisotropic stellar model. According to his findings, when the tangential pressure (p_t) adheres to the Strong Energy Condition (SEC), z_s is constrained to a maximum of 3.842. Conversely, if p_t complies with the Dominant Energy Condition (DEC), z_s can extend up to 5.211. The significance of Ivanov's proposition lies in its delineation of boundaries dictating the behavior and observable characteristics of anisotropic CSs. We have conducted a comprehensive computation of surface red-shift values (z_s) for these CSs, with detailed results provided in the accompanying table.

7 Observational constraints of mass and radius relations via $M - R$ curves

In this section, we aim to compare the behavior of compact stars in the context of $f(Q)$ gravity with existing observational results. To achieve this, we focus on the observational

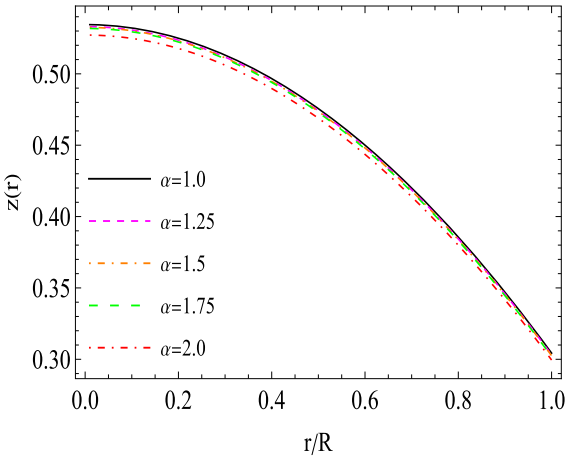

Fig. 9 The behaviour of gravitational red-shift within compact stars

measurements of three neutron star pulsars: Vela X-1 with $1.77 \pm 0.08\ M_\odot$, PSR J1614-2230 with $1.97 \pm 0.04\ M_\odot$, PSR J0952-0607 with $2.35 \pm 0.17\ M_\odot$. In the left panel of Fig. 10, we display three horizontal stripes of varying colors that represent the mass ranges of the three neutron star pulsars under consideration. Additionally, we plot the total mass M against the radius R for the compact star candidates, considering different values of the $\alpha-$parameter. The figure demonstrates that the maximum mass ($M_{\max}$) gradually rises as the values of α increase from 0.75 to 2. In our current model, Table 2 presents the predicted radii of the three neutron star pulsars based on their observed masses for various α values. The maximum masses fall within a range of approximately $1.6\ M_\odot$ to $2.6\ M_\odot$. The maximum masses correspond to radii ranging from $11.11^{+0.06}_{-0.41}$ km to $15.79^{+0.05}_{-0.09}$ km. From a theoretical standpoint, the requirement that the EoS satisfies causality, combined with our understanding of nuclear matter at low densities, suggests a loose upper limit of $m_{\max} < 2.9\ M_\odot$, as indicated by Kalogera and Baym [78] following an earlier calculation by Rhoades and Ruffini [79]. However, the maximum mass predicted by our solutions aligns well with the Rhoades-Ruffini limit of $3.2\ M_\odot$. Our analysis shows that these mass values for the three neutron star pulsars can be achieved through our proposed model of CSs in the context of $f(Q)$ gravity, utilizing various selected values of α.

From Fig. 10 (left panel), we observe that the EoS becomes stiffer as α increases. Consequently, the maximum mass supported by the corresponding EoS also rises with increasing α. To compare this with the moment of inertia (I) curve, it is essential to determine the moment of inertia. By utilizing the Bejger and Haensel formula [77], one can calculate the moment of inertia corresponding to a static solution, which is given by

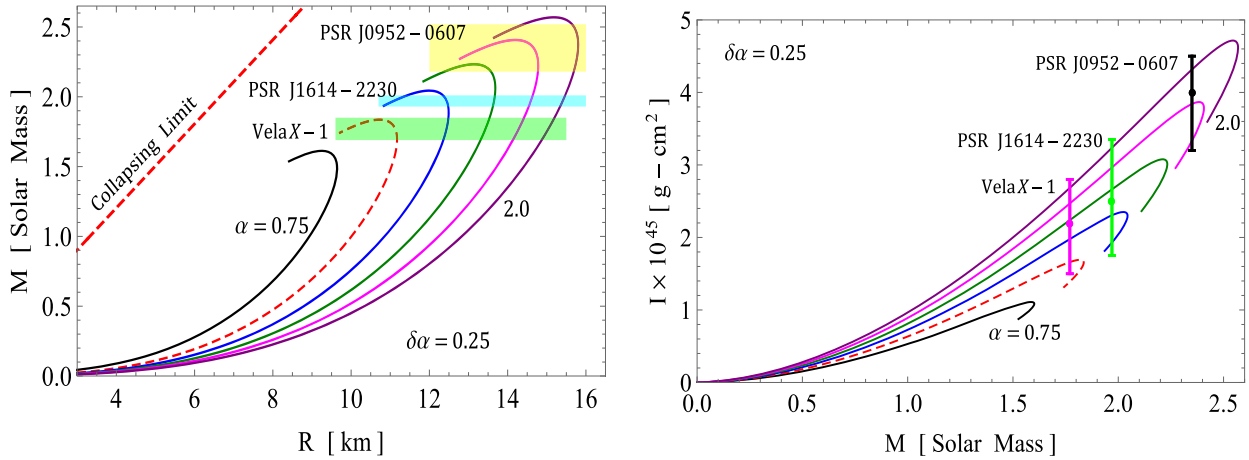

Fig. 10 Mass–radius and mass–moment of inertia relations for different values of $\alpha-$parameter

Table 2 The predicted radii of the few high masses CSs corresponding Fig. 9

Objects	$M/M_\odot$	Predicted R (km)					Predicted I ($\times 10^{45}$ g· cm^2)				
		α					α				
		1.0	1.25	1.50	1.75	2.0	1.0	1.25	1.50	1.75	2.0
Vela X-1	1.77 ± 0.08	$11.11^{+0.06}_{-0.41}$	$12.43^{+0.06}_{-0.06}$	$13.44^{+0.09}_{-0.13}$	$14.29^{+0.12}_{-0.14}$	$15.05^{+0.14}_{-0.17}$	1.65	1.97	2.23	2.46	2.67
PSR J1614-2230	1.97 ± 0.04	–	$12.46^{+0.01}_{-0.12}$	$13.65^{+0.03}_{-0.03}$	$14.60^{+0.04}_{-0.06}$	$15.41^{+0.07}_{-0.06}$	–	2.30	2.67	2.97	3.23
PSR J0952-0607	2.35 ± 0.17	–	–	–	$14.67^{+0.12}_{-}$	$15.79^{+0.05}_{-0.09}$	–	–	–	3.83	4.31

$$I = \frac{2}{5}\left(1 + \frac{(M/R)\cdot km}{M_\odot}\right) MR^2. \tag{63}$$

The $I - M$ curve is notably the most effective and sensitive to the stiffness of an EoS. As shown in the right panel of Fig. 10, the relationship between mass and moment of inertia (I) highlights this sensitivity. We can also observe that the EoS becomes progressively stiffer as α increases from 0.75 to 2. Furthermore, the transition at the peak of the $I - M$ curve is sharper than that in the $M - R$ curve. Thus, we can conclude that the sensitivity to the EoS is greater in the $I-M$ curve. Table 2 provides also the predicted moment of inertia (I) for the three neutron star pulsars in our current model, derived from their observed masses across various values of α.

8 Concluding remarks

In conclusion, this study has explored anisotropic stellar models to effectively represent CSs characterized by SS matter distributions within the modified $f(Q)$ gravity framework. By employing the linear functional form $f(Q) = \alpha Q + \beta$, we identified a significant metric potential g_{rr} and utilized a quadratic anisotropy to derive closed-form solutions to the Einstein field equations. These solutions provided valuable insights into observed pulsars, enhancing our understanding from multiple perspectives. Furthermore, we addressed the Darmois–Israel junction conditions, which play a crucial role in ensuring a seamless transition between the interior stellar models and the Schwarzschild (Anti-) de-Sitter exterior metric at the boundary. Through this approach, we successfully determined model parameters and integration constants informed by observational data from compact star Vela X-1, thereby contributing to the broader understanding of compact astrophysical object in the context of modified gravity theories. Also, the final model underwent a thorough evaluation to ensure it met the rigorous criteria for physical viability and dynamical stability within the context of $f(Q)$ gravity theory for CSs. Specifically, we assessed the regularity of the metric potentials, as well as the density, pressures, and anisotropy. We also examined the energy conditions, EoS parameters, equilibrium conditions, and stability criteria through the cracking concept, adiabatic index, and Harrison–Zeldovich–Novikov Criterion. Additionally, the model satisfied the mass-radius relationship, compactness considerations, and redshift analysis, confirming its robustness. Graphical plots generated using the specified parametric values confirmed that all the reported physical quantities aligned with established physical behavior. On the other hand, we have compared the behavior of CSs within the framework of $f(Q)$ gravity to existing observational results, focusing

on three neutron star pulsars: Vela X-1 ($1.77 \pm 0.08\ M_\odot$), PSR J1614-2230 ($1.97 \pm 0.04\ M_\odot$), and PSR J0952-0607 ($2.35 \pm 0.17\ M_\odot$). Our analysis indicates that as the α parameter increases from 0.75 to 2, the EoS becomes progressively stiffer, leading to a rise in the maximum mass supported by the EoS. We found that the maximum masses range from approximately 1.6 $M_\odot$ to 2.6 $M_\odot$, with corresponding radii between $11.11^{+0.06}_{-0.41}$ km and $15.79^{+0.05}_{-0.09}$ km. Additionally, the moment of inertia (I), calculated using the Bejger and Haensel formula, demonstrates that the $I - M$ curve is more sensitive to the stiffness of the EoS than the $M - R$ curve. This reinforces our conclusion that the sensitivity to the EoS is greater in the $I - M$ framework. Table 2 presents the predicted radii and the moment of inertia for the pulsars based on their observed masses and varying α values.

Ultimately, this investigation highlighted the significance of the physically relevant metric potential g_{rr}, the quadratic form of anisotropy, and the linear functional form $f(Q) = \alpha Q + \beta$ in developing astrophysical models that are consistent with observed phenomena.

Acknowledgements The author SKM acknowledges that this research work is supported by the TRC Project (Grant No. BFP/RGP/CBS/24/2-03). This research was funded by the Science Committee of the Ministry of Science and Higher Education of the Republic of Kazakhstan (Grant No. AP23487178). This research work was done at IUCAA, Pune (India), during RK's visit under the associate program. The author, RK, extends gratitude to IUCAA for their unwavering support and hospitality. S. K. Maurya appreciates the administration of the University of Nizwa in the Sultanate of Oman for their unwavering support and encouragement. AE thanks the National Research Foundation of South Africa for the award of a postdoctoral fellowship.

Funding There is no funding available for the publication of this research article.

Data Availability Statement This manuscript has no associated data. [Authors' comment: Data sharing is not applicable to this article as no datasets were generated or analyzed during the current study. The current work has already included a comprehensive analysis and the corresponding calculations.]

Code Availability Statement This manuscript has no associated code/software. [Authors' comment: This is a theoretical work and no new code/software has been generated. The numerical computation has been performed using Mathematica and Python.]

Declarations

Conflict of interest The authors have no relevant financial or nonfinancial interests to disclose.

Ethical statements The submitted work is original and has not been published elsewhere in any form or language (partially or in full).

Funded by SCOAP[3].

References

1. G.F.R. Ellis, R. Maartens, M.A.H. MacCallum, *Relativistic Cosmology* (Cambridge University Press, Cambridge, 2012)
2. J.B. Jiménez, L. Heisenberg, T.S. Koivisto, Universe **5**, 173 (2019)
3. J. Harada, Phys. Rev. D **101**, 024053 (2020)
4. A. Errehymy, G. Mustafa, Y. Khedif, M. Daoud, Chin. J. Phys. C **46**, 045104 (2022)
5. A.V. Astashenok, S. Capozziello, S.D. Odintsov, V.K. Oikonomou, Phys. Lett. B **811**, 135910 (2010)
6. W. Wang, H. Chen, T. Katsuragawa, Phys. Rev. D **105**, 024060 (2022)
7. A.V. Astashenok, S. Capozziello, S.D. Odintsov, V.K. Oikonomou, Phys. Lett. B **816**, 136222 (2021)
8. S.K. Maurya, A. Errehymy, B. Dayanandan, O. Donmez, K. Myrzakulov, K.S. Nisar, M. Mahmoud, JHEAp **45**, 46–61 (2025)
9. A. Errehymy, S.K. Maurya, K. Boshkayev, A.H. Abdel-Aty, H.I. Alrebdi, M. Mahmoud, Phys. Dark Universe **46**, 101622 (2024)
10. R. Kumar, S.K. Maurya, A. Errehymy, G. Mustafa, A.H. Abdel-Aty, H.I. Alrebdi, M. Mahmoud, Nucl. Phys. B **1008**, 116690 (2024)
11. S.K. Maurya, A. Errehymy, K.N. Singh, O. Donmez, K.S. Nisar, M. Mahmoud, Phys. Dark Universe **46**, 101619 (2024)
12. R. Kumar, S.K. Maurya, A. Errehymy, K. Myrzakulov, Z. Umbetova, V.N. Pathak, Chin. J. Phys. **92**, 1–22 (2024)
13. S.K. Maurya, A. Errehymy, M. Daoud, K. Myrzakulov, Z. Umbetova, Phys. Dark Universe **46**, 101586 (2024)
14. S.K. Maurya, A. Errehymy, G.E. Vîlcu, H.I. Alrebdi, K.S. Nisar, A.H. Abdel-Aty, Class. Quantum Gravity **41**(11), 115009 (2024)
15. A. Errehymy, S.K. Maurya, S. Hansraj, M. Daoud, H.I. Alrebdi, A. Abdel-Aty, Ann. Phys. **535**(8), 2300178 (2023)
16. A. Errehymy, Y. Khedif, G. Mustafa, M. Daoud, Chin. J. Phys. **77**, 1502–1522 (2022)
17. A. De Felice, S. Tsujikawa, Living Rev. Relativ. **13**, 3 (2010)
18. T.P. Sotiriou, V. Faraoni, Rev. Mod. Phys. **82**, 451 (2010)
19. S. Capozziello, M. De Laurentis, Phys. Rep. **509**, 167 (2010)
20. M. Adak, O. Sert, M. Kalay, M. Sari, Int. J. Mod. Phys. A **28**, 1350167 (2013)
21. J.B. Jiménez, L. Heisenberg, T. Koivisto, Phys. Rev. D **98**, 044048 (2018)
22. J. Beltran Jiménez, L. Heisenberg, T.S. Koivisto, J. Cosmol. Astropart. Phys. **08**, 039 (2018)
23. V. Gakis, M. Krššák, J.L. Said, E.N. Saridakis, Phys. Rev. D **101**, 064024 (2020)
24. M. Li, Y. Tong, D. Zhao, Phys. Rev. D **105**, 104002 (2022)
25. L. Mingzhe, D. Zhao, Phys. Lett. B **827**, 136968 (2022)
26. A.S. Agrawal, B. Mishra, P.K. Agrawal, Eur. Phys. J. C **83**, 113 (2023)
27. Ö. Akarsu, C. Kilinç, Astrophys. Space Sci. **326**, 315–322 (2010)
28. J. Beltran Jiménez, L. Heisenberg, T.S. Koivisto, S. Pekar, Phys. Rev. D **101**, 103507 (2020)
29. R. Lazkoz, F. Lobo, María Ortiz-Baños, V. Salzano, Phys. Rev. D **100**, 104027 (2019)

30. T. Harko, T.S. Koivisto, F.S.N. Lobo, G.J. Olmo, D. Rubiera-Garcia, Phys. Rev. D **98**, 084043 (2018)
31. F. D'Ambrosio, M. Garg, L. Heisenberg, Phys. Lett. B **811**, 135970 (2020)
32. S. Capozziello, M. Shokri, Phys. Dark Universe **37**, 101113 (2022)
33. J. Lu, X. Zhao, G. Chee, Eur. Phys. J. C **79**, 530 (2019)
34. F. Bajardi, D. Vernieri, S. Capozziello, Eur. Phys. **135**, 912 (2020)
35. S. Shekh, Phys. Dark Universe **33**, 100850 (2021)
36. T. Harko, T.S. Koivisto, F.S.N. Lobo, G.J. Olmo, D. Rubiera-Garcia, Phys. Rev. D **98**, 084043 (2018)
37. J. Lu, X. Zhao, G. Chee, Eur. Phys. J. C **79**(6), 530 (2019)
38. N. Frusciante, Phys. Rev. D **103**(4), 044021 (2021)
39. J. Estevez-Delgado, Eur. Phys. J. C **78**, 673 (2018)
40. M.L. Pattersons, A. Sulaksono, Eur. Phys. J. C **81**, 698 (2021)
41. A. Rahmansyah, A. Sulaksono, A.B. Wahidin, A.M. Setiawan, Eur. Phys. J. C **80**, 769 (2020)
42. L. Herrera, J. Ospino, A. Di Prisco, Phys. Rev. D **77**, 027502 (2008)
43. L. Herrera, W. Barreto, Phys. Rev. D **88**, 084022 (2013)
44. Z. Roupas, G.G.L. Nashed, Eur. Phys. J. C **80**, 905 (2020)
45. L. Herrera, N.O. Santos, Phys. Rep. **286**, 53 (1997)
46. J.H. Jeans, Mon. Not. R. Astron. Soc. **82**, 122 (1922)
47. G. Lemaitre, Ann. Soc. Sci. Brux. A **53**, 51 (1933)
48. R.L. Bowers, E.P.T. Liang, Astrophys. J. **188**, 657 (1974)
49. M.K. Mak, P.N. Dobson Jr., T. Harko, Int. J. Mod. Phys. D **11**(2), 207 (2002)
50. M.K. Mak, T. Harko, Proc. R. Soc. Lond. **A459**, 393 (2003)
51. M. Gleiser, K. Dev, Int. J. Mod. Phys. D **13**, 1389 (2004)
52. L. Lopes, G. Panotopoulos, A. Rincon, Eur. Phys. J. Plus **134**, 454 (2019)
53. F. Rahaman, M. Jamil, R. Sharma, K. Chakraborty, Astrophys. Space Sci. **330**, 249 (2010)
54. J.F. Sunzu, S.D. Maharaj, S. Ray, Astrophys. Space Sci. **352**, 719 (2014)
55. P. Bhar, B.S. Ratanpal, Astrophys. Space Sci. **361**, 217 (2017)
56. S.K. Maurya, Y.K. Gupta, B. Dayanandan, M.K. Jasim, A. AlAhmed, Int. J. Mod. Phys. D **26**(2), 1750002 (2017)
57. S. Thirukkanesh, R. Sharma, S.D. Maharaj, Eur. Phys. J. Plus **134**, 378 (2019)
58. G. Panotopoulos, A. Rincon, I. Lopes, Eur. Phys. J. C **81**, 63 (2021)
59. P. Bhar, Eur. Phys. J. C **83**, 737 (2023)
60. G.G.L. Nashed, S. Capoziello, Eur. Phys. J. C **81**, 481 (2021)
61. G. Mustafa, M.F. Shamir, M. Ahmed, A. Ashraf, Chin. J. Phys. **67**, 576 (2020)
62. P. Bhar, Eur. Phys. J. C **135**, 757 (2020)
63. D. Zhao, Eur. Phys. J. C **82**, 303 (2022)
64. S. Das, K. Chakraborty, F. Rahaman, S. Majumder, Eur. Phys. J. C **84**(5), 527 (2024)
65. G. Darmois, Mem. Sci. Math. Fasc. XXV **58**, 25 (1927)
66. W. Israel, Nuo. Cim. B **44**, 1 (1996)
67. S. Kaur, S.K. Maurya, S. Shukla, Phys. Scr. **98**(10), 105304 (2023)
68. R.C. Tolman, Phys. Rev. **55**(4), 364 (1939)
69. J.R. Oppenheimer, G.M. Volkoff, Phys. Rev. **55**(4), 374 (1939)
70. L. Herrera, Phys. Lett. A **165**, 206 (1992)
71. B.K. Harrison, K.S. Thorne, M. Wakano, J.A. Wheeler, *Gravitational Theory and Gravitational Collapse* (University of Chicago Press, Chicago, 1965)
72. Y.B. Zeldovich, I.D. Novikov, *Relativistic Astrophysics Stars and Relativity*, vol. 1 (University of Chicago Press, Chicago, 1971)
73. H. Knutsen, On the stability and physical properties of an exact relativistic model for a superdense star. Mon. Not. R. Astron. Soc. **232**(1), 163–174 (1988)
74. A. Di Prisco, E. Fuenmayor, L. Herrera, V. Varela, Tidal forces and fragmentation of self-gravitating compact objects. Phys. Lett. A **195**(1), 23–26 (1994)
75. A. Di Prisco, L. Herrera, V. Varela, Cracking of homogeneous self-gravitating compact objects induced by fluctuations of local anisotropy. Gen. Relativ. Gravit. **29**(10), 1239–1256 (1997)
76. B.V. Ivanov, Phys. Rev. D **65**, 104011 (2002)
77. M. Bejger, P. Haensel, Astron. Astrophys. **396**, 917 (2002)
78. V. Kalogera, G. Baym, Astrophys. J. Lett. **470**, L61–L64 (1996)
79. C.E. Rhoades Jr., R. Ruffini, Phys. Rev. Lett. **32**, 324–327 (1974)